http://dx.doi.org/10.5012/bkcs.2014.35.4.1182

Synthesis of $Cd_{1-x}Zn_xS/K_4Nb_6O_{17}$ Composite and its Photocatalytic Activity for Hydrogen Production

Yinghua Liang, Meiyi Shao, Li Liu, Jinshan Hu, and Wenquan Cui*

*College of Chemical Engineering, Hebei United University, Tangshan 063009, P.R. China. *E-mail: wkcui@163.com*
Received November 29, 2013, Accepted December 29, 2013

$Cd_{1-x}Zn_xS$-sensitized $K_4Nb_6O_{17}$ composite photocatalysts (designated $Cd_{1-x}Zn_xS/K_4Nb_6O_{17}$) were prepared *via* a simple deposition-precipitation method. The samples were characterized by X-ray diffraction (XRD), scanning electron microscopy (SEM), transmission electron microscopy (TEM), energy dispersive X-ray spectrometry (EDS), N_2 sorption, ultraviolet–visible light diffuse reflectance spectroscopy (UV–Vis DRS), photoluminescence measurements (PL), and X-ray photoelectron spectroscopy (XPS). The $Cd_{0.8}Zn_{0.2}S$ particles were scattered on the surface of $K_4Nb_6O_{17}$, and had a relatively uniform size distribution around 50 nm. The absorption edge of $K_4Nb_6O_{17}$ was shifted to the visible light region and the recombination of photo-generated electrons and holes suppressed after $Cd_{0.8}Zn_{0.2}S$ loading. The $Cd_{0.8}Zn_{0.2}S$(25 wt %)/$K_4Nb_6O_{17}$ composite possessed the highest photocatalytic activity for hydrogen production under visible light irradiation, evolving 8.278 mmol/g in 3 h. Recyclability tests were performed, and the composite photocatalysts were found to be fairly stable. The mechanism of charge separation between the photogenerated electrons and holes at the $Cd_{0.8}Zn_{0.2}S/K_4Nb_6O_{17}$ composite was discussed.

Key Words : $Cd_{0.8}Zn_{0.2}S/K_4Nb_6O_{17}$, Photocatalysis, Hydrogen evolution, Precipitation, Nanomaterials

Introduction

Hydrogen evolution from photocatalytic water splitting under solar irradiation is a prospective sustainable solution to global environmental and energy problems.[1-3] In light of this, the development of visible-light-driven photocatalysts remains a crucial issue to address for the efficient and effective production of hydrogen using solar energy.[4]

Layered semiconductors, such as $K_4Nb_6O_{17}$,[5] $K_2Ti_4O_9$,[6] $K_2La_2Ti_3O_{10}$ and $La_2Ti_2O_7$,[7-9] have been reported in literature and shown to possess high photocatalytic activities for photocatalytic water splitting. Particularly, $K_4Nb_6O_{17}$ exhibits high activity for hydrogen production from water under UV irradiation due to its unique layered structure.[10] $K_4Nb_6O_{17}$ is composed of layers of niobium oxide sheets, in which potassium ions locate in two different kinds of interlayers. One type of interlayer is easily hydrated and the K^+ ions can be exchanged with multivalent cations (Ca^{2+}, Ni^{2+}, Li^+, Na^+ ions, *etc*), and the other cannot take up water molecules and can only be exchanged with univalent cations.[11,12] Compared with TiO_2, one of the most widely used photocatalysts, the layered structure of $K_4Nb_6O_{17}$ possesses more reaction active sites, the interlamination can be modified and the photo-induced electrons can more easily migrate to the surface of catalyst to prevent the recombination of photo-generated holes and electrons, which make a contribution to the improvement of photocatalytic activities. However, the wide band gap of this material (~3.1 eV) leads to low efficiency under visible light irradiation,[13] motivating recent research in the development of visible-light-driven $K_4Nb_6O_{17}$ composite photocatalysts. Such composites have been prepared through coupling narrow band gap guest semiconductors, such as CdS,[14] PbS,[15] *etc*., into the host layered compounds to improve the visible light absorption for the composite layered semiconductors. However, the practical applications of layered structure semiconductors are still limited due to low photocatalytic efficiencies, so further work is necessary to improve the visible light response and charge separation mechanisms in these materials.

$Cd_{1-x}Zn_xS$, a solid solution of CdS and ZnS, possesses tunable composition and band gap,[16] which can be changed by adjusting the stoichiometric ratio between Zn and Cd, resulting in an observed band gap energy between that of CdS (2.4 eV) and of ZnS (3.6 eV). Therefore, the photocatalytic activity of $K_4Nb_6O_{17}$ can be improved by utilizing the sensitization effect of this $Cd_{1-x}Zn_xS$ to enhance the visible light response of $K_4Nb_6O_{17}$ and by promoting the separation of photo-induced carriers. To the best of the authors' knowledge, the photocatalytic performance over $Cd_{1-x}Zn_xS$ surface-sensitized $K_4Nb_6O_{17}$ has not yet been reported.

Herein, we report a novel nano-composite $Cd_{1-x}Zn_xS/K_4Nb_6O_{17}$ photocatalyst with high visible light activity, which was synthesized *via* a simple deposition-precipitation method by depositing the adjustable band-gap $Cd_{1-x}Zn_xS$ particles on the surface of $K_4Nb_6O_{17}$. The photocatalytic activity of the catalyst was investigated by splitting water into hydrogen under visible light irradiation, and a possible mechanism for the reaction was proposed.

Experimental

Photocatalyst Synthesis. All of the reagents were analytical grade and used without further purification. The

$K_4Nb_6O_{17}$ materials were obtained *via* a high temperature solid state method,[17] as reported in our previous research.[18] The $Cd_{1-x}Zn_xS$ sample was prepared *via* a deposition-precipitation method. In a typical synthesis, a white intermediate was precipitated by adding a mixed Cd^{2+}/Zn^{2+} aqueous solution containing appropriate molar ratios of $Cd(CH_3COO)_2{\cdot}2H_2O$ and $Zn(CH_3COO)_2{\cdot}2H_2O$ dropwise into an NaOH aqueous solution under stirring at 85 °C. The intermediate obtained was then converted to CdS/ZnS by dropwise addition of an $Na_2S{\cdot}9H_2O$ aqueous solution, containing a double excess of S^{2-} relative to the amount of metal ions present, followed by continuous stirring for 1 h. The as-produced precipitate was collected by filtration and washed with deionized water and ethanol respectively. The product was then dried at 80 °C for 12 h and subsequently calcined at 400 °C for 1 h. The CdS/ZnS samples prepared, which contained various concentrations of CdS and ZnS, were labeled as $Cd_{1-x}Zn_xS$ (where x is the molar concentration of ZnS: 0, 0.2, 0.4, 0.5, 0.6, 0.8, 1, respectively).

$Cd_{1-x}Zn_xS/K_4Nb_6O_{17}$ composites were synthesized similarly by a deposition-precipitation method using $Cd(CH_3COO)_2{\cdot}2H_2O$, $Zn(CH_3COO)_2{\cdot}2H_2O$, NaOH, $Na_2S{\cdot}9H_2O$, and $K_4Nb_6O_{17}$.

Characterization of the Photocatalysts. The crystal structures and the phases of the samples were studied by X-ray diffractometry (XRD) using a Rigaku D/MAX2500 PC diffractometer with Cu Kα radiation, with an operating voltage of 40 kV and an operating current of 100 mA. The morphologies of the samples were probed using scanning electron microscopy (SEM) (Hitachi, s-4800) and transmission electron microscopy (TEM) (Jeol ltd, JEM-2010). The chemical compositions of the sample were tested using an energy dispersive X-ray detector (EDS, Thermo Noran 7). UV-visible light (UV-vis) diffuse reflectance spectra were recorded on a UV-vis spectrometer (Puxi, UV1901), and the luminescence of the powdered samples was measured on a spectrofluorometer (Hitachi, f7000). The chemical states of the photocatalysts were analyzed by XSAM800 X-ray photoelectron spectroscopy (XPS). The Brunauer-Emmett-Teller (BET) sorption measurements were performed on a JW-BK nitrogen adsorption apparatus at 77.3 K.

The photocatalytic activities of hydrogen production for the photocatalyst samples were examined in an overhead irradiation system. Typically, 0.3 g photocatalyst powder was dispersed in a Pyrex reaction cell containing 100 mL of aqueous solution of 0.1 M Na_2S, 0.5 M Na_2SO_3 and 1 M KOH. Cooling was provided by an external cooling jacket, and the temperature of the reaction was controlled to 25 ± 2 °C. The light source used was a 300 W xenon lamp (with the light with wavelengths $\lambda < 400$ nm filtered out by a filter). The suspensions were deairated with Ar gas for 30 min prior to irradiation to prevent uptake of photo-generated electrons by dissolved oxygen. The produced hydrogen gas was detected using an online gas chromatography system (SHIMADZU-GC-2014C, molecular sieve 5 A column, TCD detector, Ar carrier). Ar gas was used as a carrier for the products.

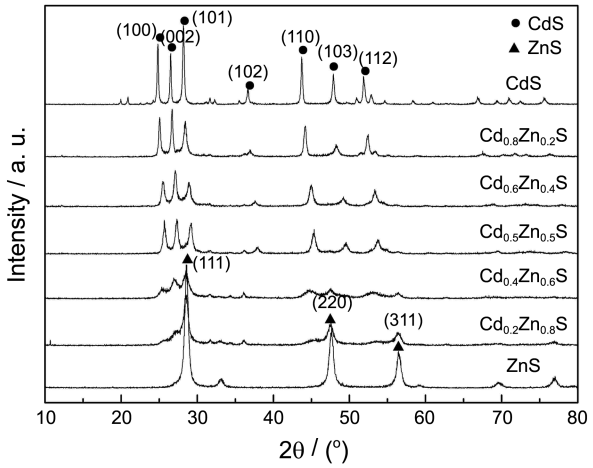

Figure 1. XRD patterns of $Cd_{1-x}Zn_xS$ solid solutions containing various molar ratios of Cd and Zn.

Results and Discussion

Catalyst Characterization. XRD patterns for $Cd_{1-x}Zn_xS$ materials prepared at various Zn molar concentrations (x-values) are shown in Figure 1. The obtained ZnS exhibited diffraction peaks at 2θ values of 28.608°, 47.589° and 56.471°, originating from the (111), (220) and (311) crystal planes of cubic zincblende ZnS (JCPDS 65-0309), respectively. The characteristic diffraction peaks for CdS were observed at 2θ of 24.807°, 26.507°, 28.182°, 36.620°, 43.681°, 47.879° and 51.880°, which were attributed to the (100), (002), (101), (102), (110), (103) and (112) crystal planes of the CdS crystal, respectively. This was indexed to hexagonal CdS (JCPDS 65-3414). The XRD spectra obtained for the $Cd_{1-x}Zn_xS$ material varied from those of CdS and ZnS. The main strong peaks in $Cd_{1-x}Zn_xS$ were shifted compared to those of pure CdS and ZnS, and the intensities were reduced. The diffraction peaks of the photocatalysts were also observed to be shifted to higher angles as the Zn molar concentrations increased. This continuous shift indicated that the resulting crystals obtained were not simple physical mixtures of CdS and ZnS particles, but were $Cd_{1-x}Zn_xS$ solid solutions. The Zn^{2+} was considered to be incorporated into the CdS lattice or to have entered its interstitial sites, since the radii of Zn^{2+} ions (0.74 Å) were smaller than those of Cd^{2+} (0.97 Å).[19-21] Moreover, the electronegativities of Cd (1.69) and Zn (1.65) were very close, which increased their likelihood of forming a solid solution.[22] According to Scherrer's equation,[23] the average crystallite size of $Cd_{0.8}Zn_{0.2}S$, $Cd_{0.5}Zn_{0.5}S$, and $Cd_{0.2}Zn_{0.8}S$ were calculated to be 15.8 nm, 10.5 nm, 8.6 nm, respectively. The size of the $Cd_{1-x}Zn_xS$ solid solution became smaller with increasing Zn concentration, which may have been due to the small radii of the Zn^{2+} ion compared to that of Cd^{2+}, which led to a decrease in the crystal lattice parameters.

The XRD patterns for $K_4Nb_6O_{17}$, $Cd_{0.8}Zn_{0.2}S$, and $Cd_{0.8}Zn_{0.2}S/K_4Nb_6O_{17}$ are given in Figure 2, respectively. The characteristic diffraction peaks for $Cd_{0.8}Zn_{0.2}S$ were

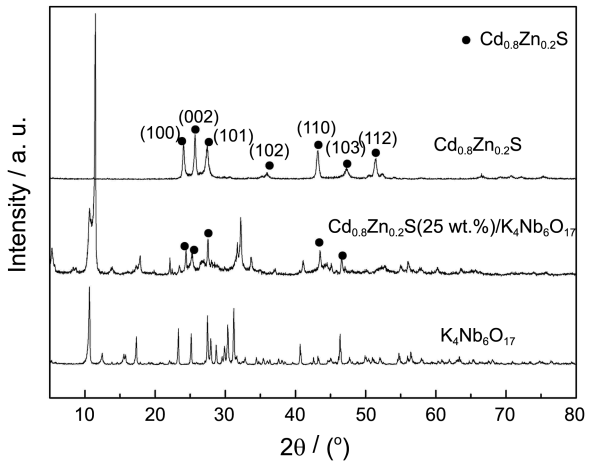

Figure 2. XRD patterns of $Cd_{0.8}Zn_{0.2}S$, $K_4Nb_6O_{17}$ and $Cd_{0.8}Zn_{0.2}S$/$K_4Nb_6O_{17}$.

observed at 2θ values of 24.835°, 26.526°, 28.203°, 36.648°, 43.737°, 47.869° and 51.871°, and were attributed to the (100), (002), (101), (102), (110), (103), and (112) crystal planes of the $Cd_{0.8}Zn_{0.2}S$ crystal, respectively, and the spectra was indexed to hexagonal $Cd_{0.8}Zn_{0.2}S$ (JCPDS 49-1302). The XRD patterns of the prepared potassium niobate were also indexed to pure phase orthorhombic $K_4Nb_6O_{17}$, according to JCPDS (31-1064). The diffraction peaks of the $Cd_{0.8}Zn_{0.2}S$ (100), (002), (101), (110) and (103) crystal planes also appeared in the XRD patterns of $Cd_{0.8}Zn_{0.2}S$/$K_4Nb_6O_{17}$ composites, suggesting that $Cd_{0.8}Zn_{0.2}S$ and $K_4Nb_6O_{17}$ were successfully synthesized and mixed together. The diffraction peaks obtained in the spectra for the $Cd_{0.8}Zn_{0.2}S$/$K_4Nb_6O_{17}$ composite were weaker than those observed in the pure $K_4Nb_6O_{17}$ pattern, indicating that the surface of $K_4Nb_6O_{17}$ was covered by $Cd_{0.8}Zn_{0.2}S$ particles.

The morphologies of the samples were observed by SEM and TEM, HRTEM and SAED, as shown in Figure 3. From the SEM images shown in Figure 3(a)-(g), the $Cd_{1-x}Zn_xS$ particles prepared with x values ranging from 0 to 1 were well developed, and exhibited a size distribution between 20 nm to 100 nm. As shown in Figure 3(a), CdS exhibited nearly spherical, well-crystallized morphology and a relatively uniform size distribution of approximately 100 nm. From Figure 3(b)-(f), the particle size was found to gradually decrease with increasing Zn content, while the morphology became increasingly irregular. The particle size of ZnS was found to be approximately 20 nm, as seen in Figure 3(g). The smaller primary ZnS nanocrystals were also observed to form huge granular aggregates. From Figure 3(b)-(g), the $Cd_{1-x}Zn_xS$ particles displayed a sheet-like morphology. This varied from that of CdS, which may have been due to an associated change in the crystal structure from hexagonal to cubic.[24] From the SEM image shown in Figure 3(h), the $K_4Nb_6O_{17}$ particles were found to exhibit a relatively uniform size distribution of approximately 1-3 μm. The morphology of the prepared $Cd_{0.8}Zn_{0.2}S$/$K_4Nb_6O_{17}$, shown in Figure 3(i), indicated that nano-$Cd_{0.8}Zn_{0.2}S$ particles were uniformly dispersed on the surface of $K_4Nb_6O_{17}$ with a size distribution within 50 nm. In addition, at a higher resolution, the TEM image shown in (Figure 3(j)) also indicated that each of these nanoparticles was in fact composed of even smaller primary nanocrystals with crystallite size of 10-20 nm, which matched well with the average crystallite size derived from the XRD data. The synthesized $Cd_{0.8}Zn_{0.2}S$/$K_4Nb_6O_{17}$ composite was also observed by HRTEM (Figure 3(j)), and the fringe spacing was found to be about 3.36 Å, which was in good agreement with the interplanar distance of the (002) plane of $Cd_{0.8}Zn_{0.2}S$, further confirming the existence of $Cd_{0.8}Zn_{0.2}S$ in the composite. The selected area electron diffraction (SAED) pattern taken from an individual particle is shown in Figure 3(m), with the presence of the ring pattern evidencing that the nanoparticles obtained were polycrystalline. Three diffraction rings corresponding to the (100), (002), (101) planes of $Cd_{0.8}Zn_{0.2}S$ were observed, respectively. The EDS spectrum obtained from the $Cd_{0.8}Zn_{0.2}S$ (25 wt %)/$K_4Nb_6O_{17}$ composite is given in Figure 3e. In this spectrum, peaks associated with O, Zn, K, Nb, S and Cd were observed, corresponding to $K_4Nb_6O_{17}$ (K, Nb, O peaks, respectively) and $Cd_{1-x}Zn_xS$ (Cd, Zn, S peaks, respectively). The EDS results confirmed that the obtained product was comprised of $K_4Nb_6O_{17}$ loaded with $Cd_{1-x}Zn_xS$. To further explore the chemical compositions of the composites, XRF analysis was employed to determine the as-prepared $Cd_{1-x}Zn_xS$ and $Cd_{0.8}Zn_{0.2}S$(25 wt %)/$K_4Nb_6O_{17}$ samples, as given in Table 1. It can be seen that the metal contents of Cd and Zn in each $Cd_{1-x}Zn_xS$ sample were slightly reduced compared to the theoretical ratio, which was similar with the reported literature.[25] For x=0(CdS catalyst) the molar ratio of Cd and S was found to be 47.68(mass %):51.15(mass %), indicating that the sample was slightly S-rich. The Cd^{2+} and Zn^{2+} ions that were not used for the formation of solid solution were thought to be washed off when XRF samples were collected. The $Cd_{0.8}Zn_{0.2}S$(25 wt %)/$K_4Nb_6O_{17}$ sample was also measured by XRF, the contents of elements Cd, Zn and S were found to be 16.55(mass %), 2.34(mass %) and 6.11(mass %), respectively, yielding a molar ratio of Cd:Zn:S of 0.77: 0.19:1, and the calculated value of $Cd_{0.8}Zn_{0.2}S$ content in the composite was 23.87%. The results confirmed that the actual loading content of $Cd_{0.8}Zn_{0.2}S$ onto the layered host material was in good agreement with the theoretical values.

The optical absorptions of the as-prepared $Cd_{1-x}Zn_xS$ samples were investigated using UV-vis diffuse reflectance spectra, and the results obtained are given in Figure 4. The absorption edge of ZnS was observed at approximately 410 nm, and the absorption edge of the $Cd_{1-x}Zn_xS$ solid solution was gradually red shifted with increasing content of Cd, with the pure CdS exhibiting an absorption edge at about 550 nm. This shift may have been caused by a band transition of the $Cd_{1-x}Zn_xS$ solid solution, which also further proved that CdS and ZnS successfully formed a solid solution. The band gaps of these samples were estimated from the onset of the absorption edges, and found to to be between 2.26 eV and 3.03 eV (for x values between 0 and 1, respectively). Therefore, the band gap position of the $Cd_{1-x}Zn_xS$ solid solution could be adjusted by adjusting the ratio of the composition

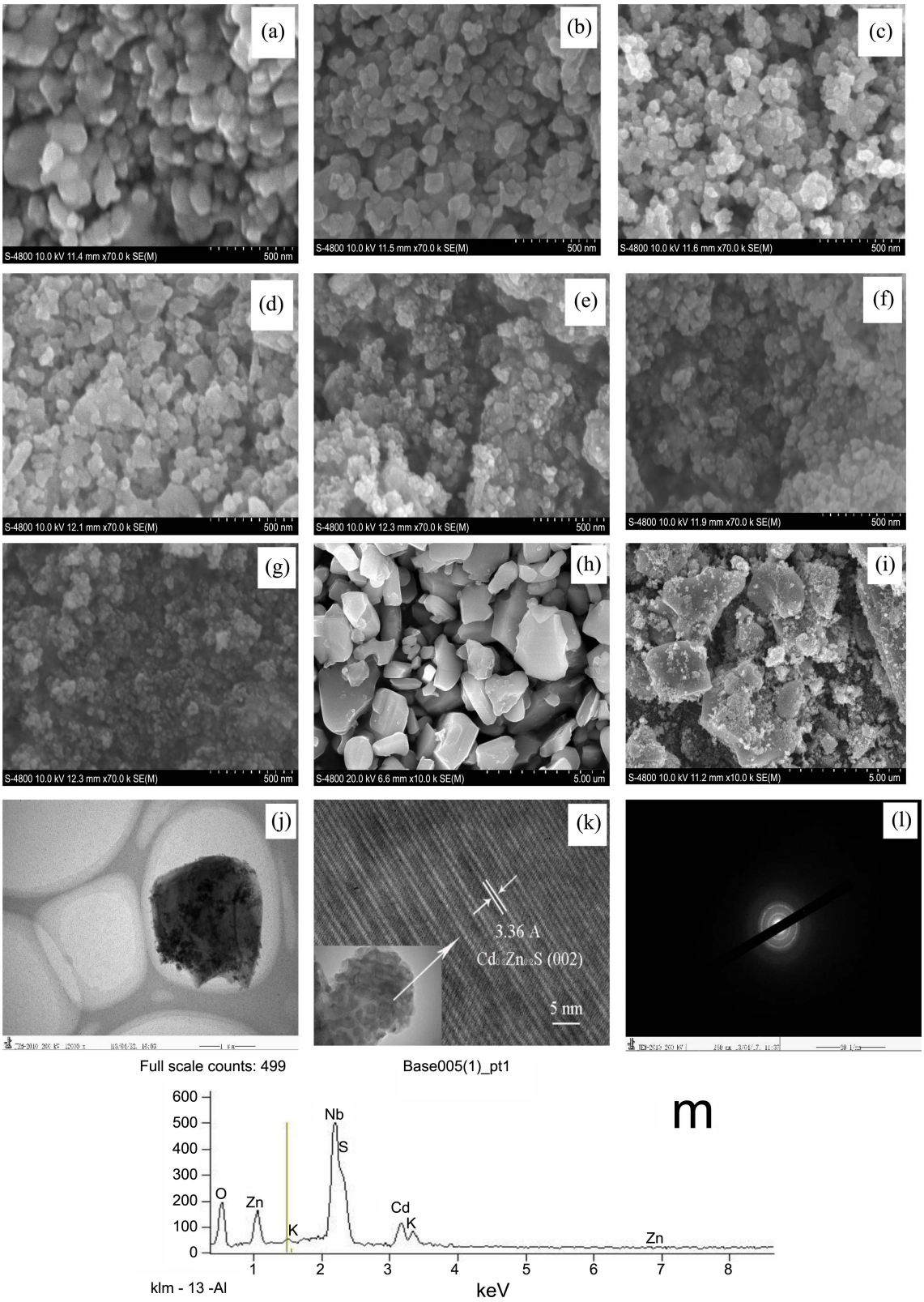

Figure 3. SEM images of prepared photocatalysts: (a) CdS, (b) $Cd_{0.8}Zn_{0.2}S$, (c) $Cd_{0.6}Zn_{0.4}S$, (d) $Cd_{0.5}Zn_{0.5}S$, (e) $Cd_{0.4}Zn_{0.6}S$, (f) $Cd_{0.2}Zn_{0.8}S$, (g) ZnS, (h) $K_4Nb_6O_{17}$, (i) $Cd_{0.8}Zn_{0.2}S$(25 wt %)/$K_4Nb_6O_{17}$; TEM and HRTEM images of $Cd_{0.8}Zn_{0.2}S$(25 wt %)/$K_4Nb_6O_{17}$ (j and k) and corresponding SAED pattern and EDS pattern (l and m).

of CdS and ZnS particles. The sharp absorption curve also implied that the absorption was almost only attributed to the band gap transition of electrons.[26]

The UV-vis diffuse reflectance spectra for various com-

Table 1. Composition of solid solutions, as measured by XRF

Stoichiometric composition	Composition observed by XRF
CdS	$Cd_{0.93}S$
$Cd_{0.8}Zn_{0.2}S$	$Cd_{0.75}Zn_{0.19}S$
$Cd_{0.6}Zn_{0.4}S$	$Cd_{0.56}Zn_{0.37}S$
$Cd_{0.5}Zn_{0.5}S$	$Cd_{0.48}Zn_{0.46}S$
$Cd_{0.4}Zn_{0.6}S$	$Cd_{0.37}Zn_{0.54}S$
$Cd_{0.2}Zn_{0.8}S$	$Cd_{0.18}Zn_{0.76}S$
ZnS	$Zn_{0.91}S$

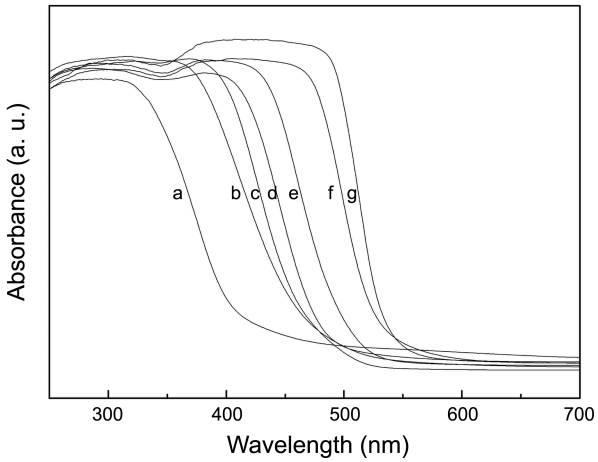

Figure 4. UV-vis diffuse reflectance spectra of prepared photocatalysts: (a) ZnS, (b) $Cd_{0.2}Zn_{0.8}S$, (c) $Cd_{0.4}Zn_{0.6}S$, (d) $Cd_{0.5}Zn_{0.5}S$, (e) $Cd_{0.6}Zn_{0.4}S$, (f) $Cd_{0.8}Zn_{0.2}S$, (g) CdS.

posite photocatalysts prepared using various weight percents of $Cd_{1-x}Zn_xS$ on $K_4Nb_6O_{17}$ are given in Figure 5. The absorption edge of $K_4Nb_6O_{17}$ was observed at approximately 400 nm, corresponding to a band gap of 3.1 eV. Therefore, most of the light absorption from the layered host material was in UV range. In contrast, the $Cd_{0.8}Zn_{0.2}S$ sample showed strong absorption in the range of $\lambda < 530$ nm, corresponding to a band gap of approximately 2.36 eV. Upon introduction of the $Cd_{0.8}Zn_{0.2}S$ into the composite, the absorption edge in the resulting materials was noticeably red-shifted to approximately 530 nm. The absorption spectra obtained for all of the prepared $Cd_{0.8}Zn_{0.2}S/K_4Nb_6O_{17}$ composites possessed this visible-light absorption, and the absorption intensity gradually increased with increasing amount of $Cd_{0.8}Zn_{0.2}S$. This indicated that the visible light absorption in the composite samples was due to distinct specimens of $Cd_{0.8}Zn_{0.2}S$, and that the external surface of $K_4Nb_6O_{17}$ was gradually covered with $Cd_{0.8}Zn_{0.2}S$. When the $Cd_{0.8}Zn_{0.2}S$ loading content reached 30 wt %, the absorption inflection due to $K_4Nb_6O_{17}$ was less noticeable, indicating that most of the $K_4Nb_6O_{17}$ surface was covered by $Cd_{0.8}Zn_{0.2}S$ nanoparticles.

Molecular fluorescence spectroscopy is a kind of emission spectrum caused by electron-hole recombination, which can reflect the migration and capture of photo-induced carriers.[27] The results obtained for the prepared $Cd_{1-x}Zn_xS$ samples are given in Figure 6(a). The emission peak exhibited more or less sharp peaks at 434, 468, 488, 514, 548 nm, respectively. It can be seen that, for each sample, the PL peak energy was

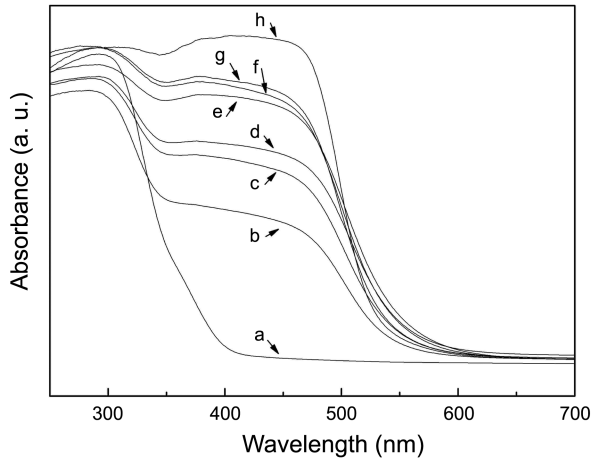

Figure 5. UV-vis diffuse reflectance spectra of prepared photocatalysts: (a: $K_4Nb_6O_{17}$, b: $Cd_{0.8}Zn_{0.2}S$(5 wt %)/$K_4Nb_6O_{17}$, c: $Cd_{0.8}Zn_{0.2}S$ (10 wt %)/$K_4Nb_6O_{17}$, d: $Cd_{0.8}Zn_{0.2}S$(15 wt %)/$K_4Nb_6O_{17}$, e: $Cd_{0.8}Zn_{0.2}S$ (20 wt %)/$K_4Nb_6O_{17}$, f: $Cd_{0.8}Zn_{0.2}S$(25 wt %)/$K_4Nb_6O_{17}$, g: $Cd_{0.8}Zn_{0.2}S$ (30 wt %)/$K_4Nb_6O_{17}$, h: pure $Cd_{0.8}Zn_{0.2}S$).

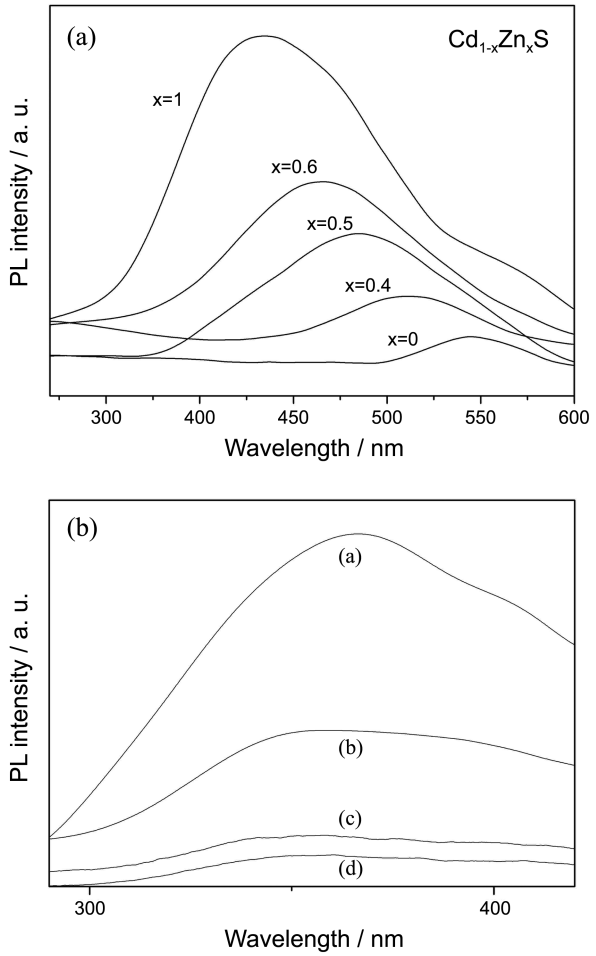

Figure 6. Fluorescence spectra of photocatalysts (λ_{ex} = 250 nm): a: $Cd_{1-x}Zn_xS$; b: (a) $K_4Nb_6O_{17}$; (b) $Cd_{0.8}Zn_{0.2}S$ (5 wt %)/$K_4Nb_6O_{17}$; (c) $Cd_{0.8}Zn_{0.2}S$ (15 wt %)/$K_4Nb_6O_{17}$; (d) $Cd_{0.8}Zn_{0.2}S$ (25 wt %)/$K_4Nb_6O_{17}$.

consistently lower than its corresponding band gap due to the direct transition between valence band and conduction band, which indicated that the radiative transition occurred from the surface states rather than the excitation transition.[28] Moreover, the broad PL peaks obtained shifted toward higher energies with increasing Cd content, due to the formation of nanocrystalline $Cd_{1-x}Zn_xS$ solid solutions. The shift of emission peak was thought to be attributable to the changes in surface structure as the Zn substituted Cd in the CdS lattice, influencing the emission from surface defects.

As shown in Figure 6(b), the pure $K_4Nb_6O_{17}$ exhibited an excitation peak around 370 nm. Compared to pure $K_4Nb_6O_{17}$, the positions of the emission peaks of $Cd_{0.8}Zn_{0.2}S/K_4Nb_6O_{17}$ composites were hardly shifted, indicating that the emission was due to $K_4Nb_6O_{17}$ in the composite. However, the emission intensity was drastically decreased. This may be have been due to the transition of photo-induced electrons from the CB to VB in the bulk $K_4Nb_6O_{17}$ being inhibited and the recombination of electron-hole pairs suppressed due to the $Cd_{0.8}Zn_{0.2}S$ loading. This also suggested that the energy bands of $K_4Nb_6O_{17}$ and $Cd_{0.8}Zn_{0.2}S$ were coupled upon $Cd_{0.8}Zn_{0.2}S$ loading, and that the $K_4Nb_6O_{17}$ and $Cd_{0.8}Zn_{0.2}S$ particles were not physically mixed. Moreover, the intensity of the emission peak decreased as the loading amount of $Cd_{0.8}Zn_{0.2}S$ increased, which may have been because an increased $Cd_{0.8}Zn_{0.2}S$ amount would have increased the probability of transfer for the excited electrons from the $K_4Nb_6O_{17}$.[29, 30]

X-ray photoelectron spectroscopy (XPS) analysis was carried out to study the chemical states of the surface elements of the synthesized samples. The XPS spectra of Nb 3d, Cd 3d, Zn 2p, and S 2p are given in Figures 7-10. As given in Figure 7, the binding energy of Nb 3d5/2 and Nb 3d 3/2 for $K_4Nb_6O_{17}$ appeared at 206.35 eV and 208.75 eV, respectively. After $Cd_{0.8}Zn_{0.2}S$ loading onto $K_4Nb_6O_{17}$, the binding energy of Nb 3d5/2 and Nb 3d3/2 for $K_4Nb_6O_{17}$ increased to 207.05 eV and 209.5 eV, respectively. However, the binding energies of Cd 3d, Zn 2p and S 2p for $Cd_{0.8}Zn_{0.2}S/K_4Nb_6O_{17}$ were all lower than those observed for pure $Cd_{0.8}Zn_{0.2}S$. Therefore, chemical bonds were formed between the $Cd_{0.8}Zn_{0.2}S$ and $K_4Nb_6O_{17}$, leading to the variation of these binding energies of Nb, Cd, Zn and S,

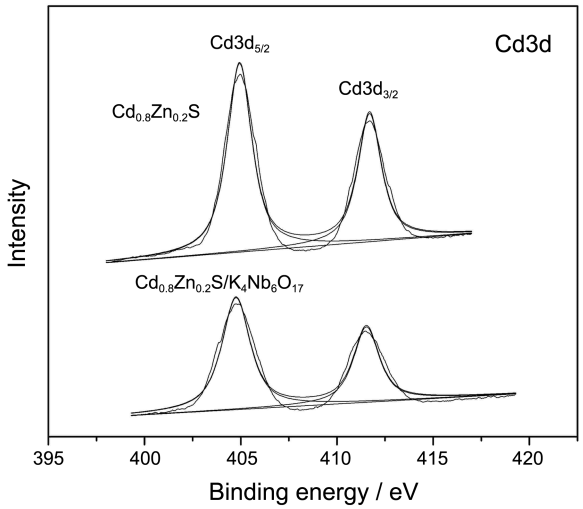

Figure 8. Cd XPS spectra for various samples.

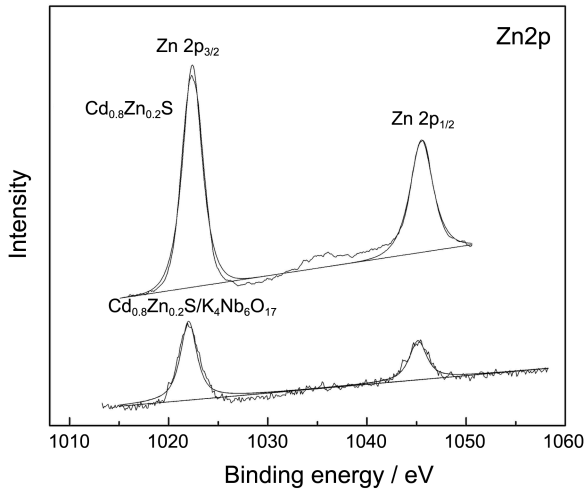

Figure 9. Zn XPS spectra for various samples.

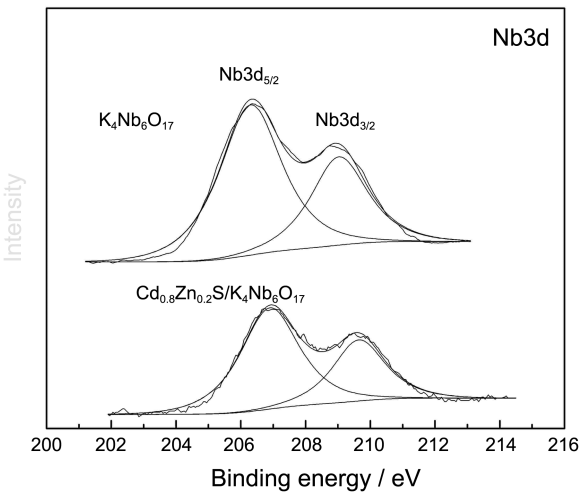

Figure 7. Nb XPS spectra for various samples.

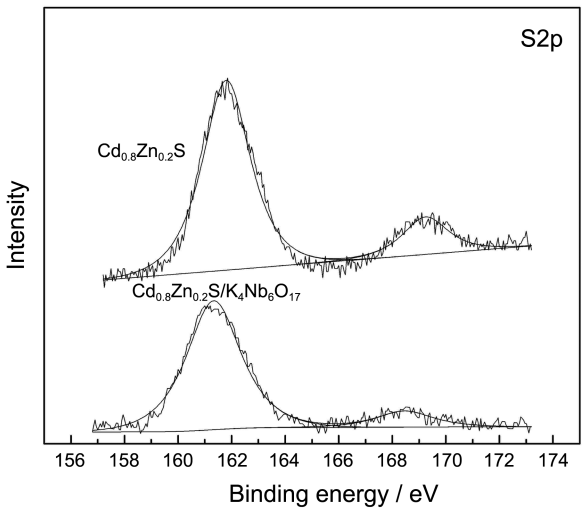

Figure 10. S XPS spectra for various samples.

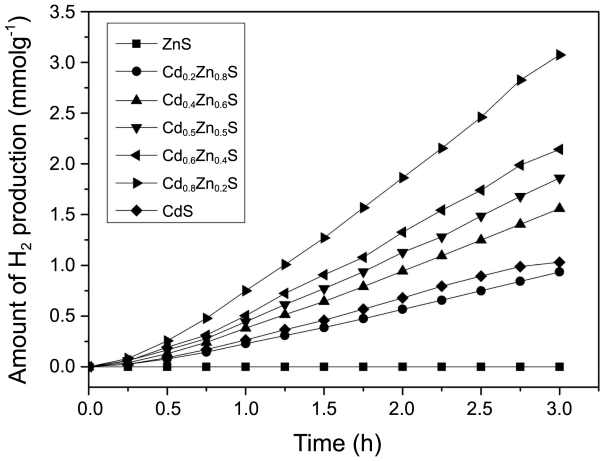

Figure 11. Photocatalytic activity for hydrogen evolution under visible light irradiation using $Cd_{1-x}Zn_xS$ samples with various values of x (zinc concentration).

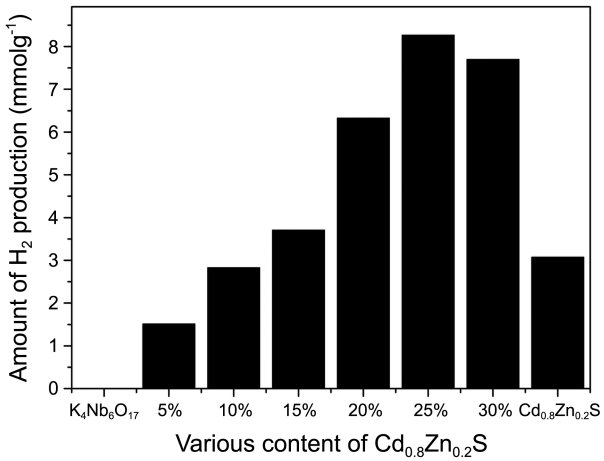

Figure 12. Photocatalytic activity for hydrogen production under visible light using $Cd_{0.8}Zn_{0.2}S/K_4Nb_6O_{17}$ photocatalysts prepared at various loadings.

respectively.[31] As the electronegativities of Cd and Zn were higher than that of Nb, the surrounding electronic density of Nb atoms in $Cd_{0.8}Zn_{0.2}S/K_4Nb_6O_{17}$ decreased, and the shielding effect became weaker, which led to the increase in the binding energy of Nb 3d.[32] Hence, with the increase of the surrounding electronic density of the Cd, Zn and S atoms of $Cd_{0.8}Zn_{0.2}S$ in the composite, the binding energy became lower. This also indicated that the ions diffused between $Cd_{0.8}Zn_{0.2}S$ and $K_4Nb_6O_{17}$ in the $Cd_{0.8}Zn_{0.2}S/K_4Nb_6O_{17}$ composite, and a solid solution was formed.

Photocatalytic Activities for Hydrogen Production. The photocatalytic activities of $Cd_{1-x}Zn_xS$ samples prepared with various zinc concentrations (x-values) were investigated for hydrogen evolution under visible light irradiation, and the results are shown in Figure 11. After 3 h of visible light irradiation, hydrogen generation was not observed in the presence of pure ZnS, indicating that ZnS was not active for photocatalytic hydrogen evolution under visible light, in accordance with its UV-vis diffuse reflectance spectra. The activity of CdS was also low, and the hydrogen production was about 1.031 mmol/g in three hours. In contrast, the $Cd_{0.8}Zn_{0.2}S$ showed high photocatalytic activity, with a photocatalytic hydrogen evolution of 3.074 mmol/g under visible light irradiation in three hours. As shown in Figure 11, the final hydrogen evolution observed in the presence of the $Cd_{0.2}Zn_{0.8}S$ solid solution was 0.935 mmol/g, which was much lower than that of $Cd_{0.8}Zn_{0.2}S$, suggesting that dissolution of CdS and ZnS may have occurred, and that the composition of the solid solution prepared with an x-value of 0.2 was significant for the high activity of photocatalytic hydrogen evolution observed. The photocatalytic activity of the solid solutions gradually decreased as the Cd/Zn molar ratio decreased, and it was thought that the addition of wide bandgap catalyst, such as ZnS, to that of CdS decreased the extent of light absorbed. This was considered disadvantageous in terms of light absorption of the photocatalyst. Additionally, for the $Cd_{1-x}Zn_xS$ solid solution, the conduction band potentials were thought to be more negative as the value of x increased.[33]

The photocatalytic performance of $Cd_{0.8}Zn_{0.2}S/K_4Nb_6O_{17}$ samples prepared at various $Cd_{0.8}Zn_{0.2}S$ loadings were evaluated by measuring photocatalytic hydrogen evolution under visible light irradiation for 3 h. As shown in Figure 12, no H_2 was detected using pure $K_4Nb_6O_{17}$ under visible light irradiation, while all of the $Cd_{0.8}Zn_{0.2}S/K_4Nb_6O_{17}$ samples exhibited higher photocatalytic activities than that of pure $K_4Nb_6O_{17}$, due to the enhancement of activity upon $Cd_{0.8}Zn_{0.2}S$ loading. This improved activity was thought to be attributable to various factors. Firstly, loading $Cd_{0.8}Zn_{0.2}S$ onto $K_4Nb_6O_{17}$ was found to enlarge the catalyst surface area according to the results of BET measurements, where the pure $K_4Nb_6O_{17}$ and $Cd_{0.8}Zn_{0.2}S/K_4Nb_6O_{17}$ possessed BET surface areas of 0.91 m^2/g and 8.693 m^2/g, respectively. Secondly, the band gaps of $K_4Nb_6O_{17}$ and $Cd_{0.8}Zn_{0.2}S$ were thought to be coupled in the composite, which may have improved the separation of electron-hole pairs, as discussed in subsequent sections. The $Cd_{0.8}Zn_{0.2}S$ loading amount also influenced the photocatalytic performance, and a suitable content of $Cd_{0.8}Zn_{0.2}S$ particles was necessary to obtain a fine particle dispersion on the surface of $K_4Nb_6O_{17}$. However, too little $Cd_{0.8}Zn_{0.2}S$ on the surface would lead to limited visible light absorption capability of the composite, while excessive loading would form overlapping particle agglomerates and shade the active sites on the surface of $K_4Nb_6O_{17}$. Based on these considerations, and from the results given in Figure 12, the $Cd_{0.8}Zn_{0.2}S$(25 wt %)/$K_4Nb_6O_{17}$ composite was found to exhibit the highest activities for photocatalytic hydrogen evolution, producing about 8.278 mmol/g hydrogen in 3 h under visible light irradiation. Therefore, 25 wt % was thought to represent an optimum $Cd_{0.8}Zn_{0.2}S$ loading onto the layered $K_4Nb_6O_{17}$.

Stability is an important parameter for photocatalysts. To evaluate the catalyst stability, we performed repeated runs for the photocatalytic activity over 0.3 g of $Cd_{0.8}Zn_{0.2}S$(25 wt %)/$K_4Nb_6O_{17}$, recovering the photocatalyst between runs. As shown in Figure 13, after five cycles, the photocatalytic

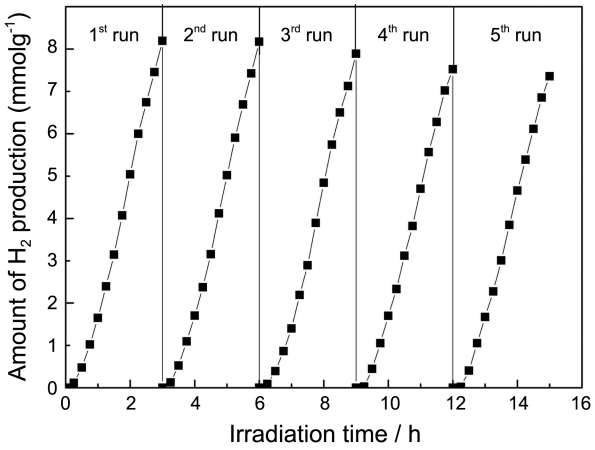

Figure 13. Repeated runs of photocatalysis over recycled sample 0.3 g of $Cd_{0.8}Zn_{0.2}S$(25 wt %)/$K_4Nb_6O_{17}$ in 0.1 M Na_2S, 0.5 M Na_2SO_3, and 1 M KOH under visible light.

activity for hydrogen evolution was maintained, suggesting that the $Cd_{0.8}Zn_{0.2}S$(25 wt %)/$K_4Nb_6O_{17}$ composite possessed good stability for repeated use in photocatalytic reactions.

Some $Cd_{0.8}Zn_{0.2}S$ composite have already been studied before, MWCNTs/$Cd_{0.8}Zn_{0.2}S$ was prepared by Liu, *etc*,[34] 15 wt % MWCNTs/$Cd_{0.8}Zn_{0.2}S$ showed the highest photocatalytic hydrogen production rate and producing 1.17 $mmol\cdot g^{-1}\cdot h^{-1}$ H_2 under visible light irradiation. Macias-Sanchez, *etc*[35] synthesized $Cd_{1-x}Zn_xS$/SBA-16 and studied the visible light photocatalytic activity for water splitting, the result showed that the $Cd_{0.8}Zn_{0.2}S$/S16 possessed the highest hydrogen evolution rate and generating 0.98 $mmol\cdot g^{-1}\cdot h^{-1}$ H_2. Li *etc*[36] prepared $Cd_{0.5}Zn_{0.5}S$/NiS photocatalyst, with the H_2 evolution rate reaching 2.32 $mmol\cdot g^{-1}\cdot h^{-1}$. However, the photocataytic for hydrogen evolution for the present work of $Cd_{0.8}Zn_{0.2}S$ (25 wt %)/$K_4Nb_6O_{17}$ was 2.76 $mmol\cdot g^{-1}\cdot h^{-1}$, which exhibited higher photocatalytic activity than the materials mentioned above, indicating that the band gaps of $Cd_{0.8}Zn_{0.2}S$ and $K_4Nb_6O_{17}$ coupled well and offered an increased probability of separation of electron and hole pairs.

Mechanistic Analysis. The $Cd_{0.8}Zn_{x0.2}S/K_4Nb_6O_{17}$ composites prepared possessed excellent activity for hydrogen evolution under visible light irradiation, and the photocatalytic mechanisms were analyzed considering the transition of the photo-induced charge carriers in the composite. Specifically, using two semiconductors in contact with different redox energy levels of their CB and VB enhanced the the efficiency of separation of photo generated carriers and also enhanced the interfacial charge transfer.

As shown in Scheme 1, according to the relative positions of the valence and conduction bands of $K_4Nb_6O_{17}$ and $Cd_{0.8}Zn_{0.2}S$, respectively, when irradiated by visible light, the $Cd_{0.8}Zn_{0.2}S$ solid solution absorbed photons and promoted electrons from its valence band to its conduction band to form the electron-hole pairs. The electric field at the $Cd_{0.8}Zn_{0.2}S/K_4Nb_6O_{17}$ interface was thought to then push the photo-generated electrons toward the conduction band of $K_4Nb_6O_{17}$, which caused the electrons to further migrate into

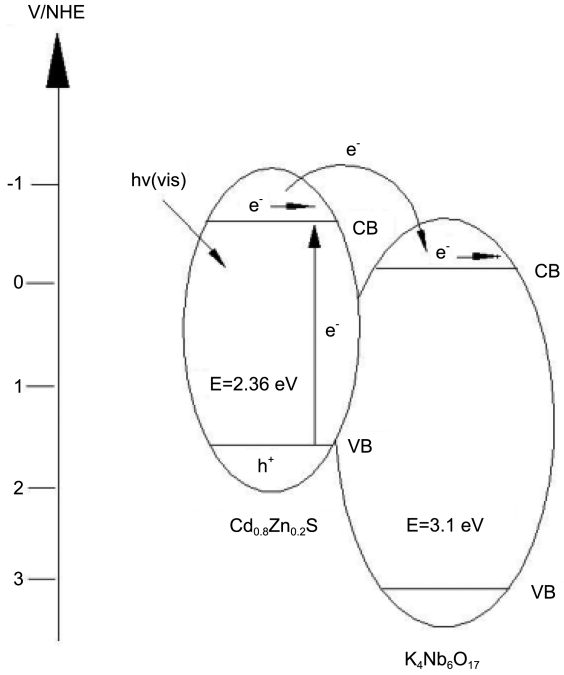

Scheme 1. Schematic illustration of electron-hole transfer under visible light.

the inner surface of the layered structure of $K_4Nb_6O_{17}$,[37] while the photo-generated holes remained on the valence band of $Cd_{0.8}Zn_{0.2}S$. As a result, the photogenerated electron-hole pairs were effectively separated and the probability of electron-hole recombination was reduced.

In the absence of sacrificial reagents, hydrogen was generated in the photocatalytic process and the catalyst consumed by photoexcited holes, as shown in Eqs. (1)-(3). However, when S^{2-} and SO_3^{2-} were utilized, various reactions occurred for the photoexcited holes, as detailed in Eqs. (4)-(7).[38]

$$Cd_{1-x}Zn_xS + h\nu \xrightarrow{visible-light} h^+ + e^- \quad (1)$$

$$S^{2-} + 2h^+ \rightarrow S \quad (2)$$

$$2e^- + 2H_2O \rightarrow H_2 + 2OH^- \quad (3)$$

$$2S^{2-} + 2h^+ \rightarrow S_2^{2-} \quad (4)$$

$$SO_3^{2-} + H_2O + 2h^+ \rightarrow SO_4^{2-} + 2H^+ \quad (5)$$

$$S_2^{2-} + SO_3^{2-} \rightarrow S_2O_3^{2-} + S^{2-} \quad (6)$$

$$S^{2-} + SO_3^{2-} + 2h^+ \rightarrow \rightarrow S_2O_3^{2-} \quad (7)$$

In this case, photoexcited holes reacted with S^{2-} and SO_3^{2-}, respectively. The SO_2^{2-} ions produced could then act as an optical filter and electron acceptor, capturing the photogenerated electrons. However, this pathway was efficiently suppressed by mixing with SO_3^{2-} ions, causing ionic $S_2O_3^{2-}$ and S^{2-} to be produced (6). Therefore, the overall process was represented by the main reaction shown in Eq. (7). As the major reaction product, $S_2O_3^{2-}$ was assumed to have little negative impact on the reaction. Based on this analysis, the sacrificial reagents were thought to be transformed into

$S_2O_3^{2-}$ as the photocatalytic reaction proceeded.

Conclusion

$Cd_{1-x}Zn_xS/K_4Nb_6O_{17}$ composite photocatalysts were successfully prepared by a facile deposition-precipitation method. The $Cd_{1-x}Zn_xS/K_4Nb_6O_{17}$ composites exhibited strong visible light absorption and displayed enhanced photocatalytic performance for hydrogen evolution under visible light irradiation. The $Cd_{0.8}Zn_{0.2}S$(25 wt %)/$K_4Nb_6O_{17}$ photocatalyst exhibited the highest photocatalytic activity under visible light irradiation, and the hydrogen evolution was 8.278 mmol/g after 3 h. This enhanced activity was thought to be due to the increase in surface area of the composite relative to the pure layered material alone. Additionally, the band gaps of $K_4Nb_6O_{17}$ and $Cd_{1-x}Zn_xS$ were coupled in the composite, which improved the separation of electron-hole pairs.

Acknowledgments. This work was supported by the National Natural Science Foundation of China (grant No. 51172063, 51202056, 51372068), Herbei Natural Science Funds for Distinguished Young Scholar (grant No. B2014209304), and the Hebei Joint Research Fund for Iron and Steel (grant No. B2014209314).

References

1. Fujishima, A.; Honda, K. *Nature* **1972**, *238*, 37.
2. Khan, S.; Al-shahry, M.; Ingler, W. B., Jr. *Science* **2002**, *297*, 2243.
3. Kudo, A.; Miseki, Y. *Chem. Soc. Rev.* **2009**, *38*, 253.
4. Zou, Z. G.; Ye, J. H.; Sayama, K.; Arakawa, H. *Nature* **2001**, *414*, 625.
5. Maeda, K.; Eguchi, M.; Youngblood, W. J.; Mallouk, T. E. *Chem. Mater.* **2008**, *20*, 6770.
6. Allen, M. R.; Thibert, A.; Sabio, E. M.; Browning, N. D.; Larsen, D. S.; Osterloh, F. E. *Chem. Mater.* **2010**, *22*, 1220.
7. Kumar, V.; Govind; Uma, S. J. *Hazard. Mater.* **2011**, *189*, 502.
8. Meng, F.; Li, J. T.; Hong, Z. L.; Zhi, M. J.; Sakla, A.; Xiang, C. C. Wu, N. Q. *Catal. Today* **2013**, *199*, 48.
9. Meng, F.; Hong, Z. L.; Arndt, J.; Li, M.; Zhi, M. J.; Yang, F.; Wu, N. Q. *Nano Research* **2012**, *5*, 213.
10. Lin, H. Y.; Lee, T. H.; Sie, C. Y. *Int. J. Hydrogen Energy* **2008**, *33*, 4055.
11. Domen, K.; Kudo, A.; Shibata, M.; Tanaka, A.; Maruya, K.; Onishi, T. *J. Chem. Soc., Chem. Commun.* **1986**, *23*, 1706.
12. Kudo, A.; Tanaka, A.; Domen, K.; Aika, K.; Onishi, T. *J. Cata.* **1988**, *111*, 67.
13. Koinuma, M.; Seki, H.; Matsumoto, Y. J. *Electroanal. Chem.* **2002**, *531*, 81.
14. Liang, Y. H.; Shao, M. Y.; Cui, W. Q.; Liu, L.; McEvoy, J. G. *J. Mol. Catal. A: Chem.* **2013**, *370*, 87.
15. Cui, W. Q.; Shao, M. Y.; Liu, L.; Liang, Y. H.; Rana, D. *Appl. Surf. Sci.* **2013**, *276*, 823.
16. Xing, C. J.; Zhang, Y. J.; Yan, W.; Guo, L. J. *Int. J. Hydrogen Energy* **2006**, *31*, 18.
17. Zhang, P.; Gao, L. J. *Colloid Interface Sci.* **2004**, *272*, 99.
18. Cui, W. Q.; Liu, Y. F.; Liu, L.; Hu, J. S.; Liang, Y. H. *Appl. Catal. A: Gen.* **2012**, *417-418*, 111.
19. Li, M. T.; Jiang, J. G.; Guo. L. J. *Int. J. Hydrogen Energy* **2010**, *35*, 7036.
20. Wang, L.; Wang, W. Z.; Shang, M.; Yin, W. Z.; Sun, S. M.; Zhang, L. *Int. J. Hydrogen Energy* **2010**, *35*, 19.
21. Xing, C. J.; Zhang, Y. J.; Yan, W.; Guo. L. J. *Int. J. Hydrogen Energy* **2006**, *31*, 2018.
22. Dean, J. A. *Lange's Handbook of Chemistry*; McGraw-Hill Book Co.: Beijing, 1999.
23. Cullit, B. D. *Elements of X-ray Diffraction*, 2nd ed.; Addision Wesley: London, 1978.
24. Mariappan, R.; Ragavendar, M.; Ponnuswamy, V. J. *Alloys Compd.* **2011**, *509*, 7337.
25. Chen, J. B.; Lin, S.; Yan, G. Y. *Catal. Commun.* **2008**, *9*, 65-69.
26. Xing, C. J.; Zhang, Y. J.; Yan, W.; Guo, L. J. *Int. J. Hydrogen Energy* **2006**, *31*, 2018.
27. Chen, H. W.; Young, K.; Kuo, Y. L. *Water Res.* **2007**, *41*, 2067.
28. Zhang, Y. C.; Chen, W. W.; Hu, X. Y. *Cryst. Growth Des.* **2007**, *7*, 580.
29. Xiao, Q.; Zhang, J.; Xiao, C.; Tan, X. K. *Catal. Commun.* **2008**, *9*, 1247-1253.
30. Wang, Q. Q.; Lin, B. Z.; Xu, B. H.; Xiao, L. L.; Chen, Z. J.; Pian, X. T. *Microporous Mesoporous Mater.* **2010**, *130*, 344-351.
31. Huo, Y. N.; Yang, X. L.; Zhu, J. *Appl. Catal. B: Environ.* **2011**, *106*, 69.
32. Huang, B. C.; Yang, Y.; Chen, X. S.; Ye, D. Q. *Catal. Commun.* **2011**, *11*, 844.
33. Wang, L.; Wang, W. Z.; Shang, M.; Yin, W. Z.; Sun, S. M.; Zhang, L. *Int. J. Hydrogen Energy* **2010**, *35*, 19.
34. Liu, X. J.; Zeng, P.; Peng, T. Y.; Zhang, X. H.; Deng, K. J. *Int. J. Hydrogen Energy* **2012**, *37*, 1375-1384.
35. Macias-Sanchez, S. A.; Nava, R.; Hernandez-Morales, V.; Acosta-Silva, Y. J.; Pawelec, B. *Int. J. Hydrogen Energy* **2013**, *38*, 11799-11810.
36. Li, N.; Zhou, B. Y.; Guo, P. H.; Zhou, J. C.; Jing, D. W. *Int. J. Hydrogen Energy* **2013**, *38*, 11268-11277.
37. Domen, K.; Ebina, Y.; Sekine, T.; Tanaka, A.; Kondo, J.; Hirose, C. *Catal. Today* **1993**, *16*, 479.
38. Bao, N. Z.; Shen, L. M.; Takata, T.; Domen, K. *Chem. Mater.* **2008**, *20*, 110.